ADVANCED MATERIALS
www.advmat.de

Highly Efficient Perovskite-Quantum-Dot Light-Emitting Diodes by Surface Engineering

Jun Pan, Li Na Quan, Yongbiao Zhao, Wei Peng, Banavoth Murali, Smritakshi P. Sarmah, Mingjian Yuan, Lutfan Sinatra, Noktan M. Alyami, Jiakai Liu, Emre Yassitepe, Zhenyu Yang, Oleksandr Voznyy, Riccardo Comin, Mohamed N. Hedhili, Omar F. Mohammed, Zheng Hong Lu, Dong Ha Kim, Edward H. Sargent, and Osman M. Bakr**

Lead halide perovskites have recently emerged as promising candidate materials for optoelectronic applications such as photovoltaics,[1–3] lasing,[4–6] and photodetectors[7–9] due to their size-tunable optical bandgaps, attractive absorption, narrow emission, and extraordinary charge-transport properties. These impressive characteristics have also triggered intense interest in applying perovskites to the field of light-emitting diodes (LEDs).[10] However, perovskite LEDs (PeLEDs) still exhibit overall low performance in comparison to other materials technologies, such as Cd-based quantum dots (QDs).[11–13] Moreover, recent advances in integrating lead halide perovskites in PeLEDs have been mainly limited to hybrid organic–inorganic perovskites such as $CH_3NH_3PbBr_3$.[14,15] The highest performance so far achieved was obtained for a green PeLED with $CH_3NH_3PbBr_3$ using a self-organized conducting polymer anode exhibiting a current efficiency of 42.9 cd A^{-1} and an external quantum efficiency (EQE) of up to 8.53%.[16] Unfortunately, such hybrid organic–inorganic perovskite materials and their resultant devices are hampered by their limited stability.[17–19]

Dr. J. Pan, W. Peng, Dr. B. Murali, Dr. S. P. Sarmah, L. Sinatra, N. M. Alyami, J. Liu, Prof. O. F. Mohammed, Prof. O. M. Bakr
Division of Physical Science and Engineering
King Abdullah University of Science and Technology
Thuwal 23955-6900, Kingdom of Saudi Arabia
E-mail: osman.bakr@kaust.edu.sa

Dr. L. N. Quan, Dr. M. Yuan, Dr. E. Yassitepe, Dr. Z. Yang, Dr. O. Voznyy, Dr. R. Comin, Prof. E. H. Sargent
Department of Electrical and Computer Engineering
University of Toronto
10 King's College Road, Toronto, Ontario M5S 3G4, Canada
E-mail: ted.sargent@utoronto.ca

Dr. L. N. Quan, Prof. D. H. Kim
Department of Chemistry and Nano Science
Ewha Woman's University
52, Ewhayeodae-gil, Seodaemun-gu, Seoul 03760, Korea

Dr. Y. Zhao, Prof. Z. H. Lu
Department of Materials Science and Engineering
University of Toronto
184 College Street, Toronto, Ontario M5S 3E4, Canada

Dr. M. N. Hedhili
Imaging and Characterization Laboratory
King Abdullah University of Science and Technology
Thuwal 23955-6900, Kingdom of Saudi Arabia

DOI: 10.1002/adma.201600784

All-inorganic perovskite QDs (APQDs), such as $CsPbX_3$ (X = Cl, Br, and I), exhibit superior thermal stability compared to their hybrid analogues. They have the potential to be integrated into various optoelectronic devices that can exploit quantum confinement effects. Kovalenko and co-workers fabricated $CsPbX_3$ QDs with exceptionally tunable optical properties and high photoluminescence (PL) quantum yield, suggesting a major opportunity to employ this family of materials for LEDs.[20] Unfortunately, the highest EQE reported so far is 0.19%,[21] which is partly since the QDs are capped with relatively insulating long ligands that are required for the processing and stability of the QDs.[22,23] Replacing these long ligands (usually oleylamine (OAm) and oleic acid (OA)) with shorter ligands without degrading or destabilizing the APQD films remains the key challenge preventing the fabrication of efficient LEDs from APQDs.

Here, we realize highly stable films of $CsPbX_3$ QDs capped with a halide ion pair (e.g., di-dodecyl dimethyl ammonium bromide (DDAB)), a relatively short ligand that facilitates carrier transport in the QD film and ultimately enables us to fabricate efficient PeLEDs. The synthesis of these films was only possible through the design of a ligand-exchange strategy that includes an intermediate step to desorb protonated OAm, which otherwise would result in the degradation of APQDs through a direct conventional ligand-exchange route. As a result of our novel ligand-exchange strategy, we were able to utilize halide-ion-pair-capped $CsPbBr_3$ QDs in green PeLEDs with a device structure of indium tin oxide (ITO)/poly(ethylene dioxythiophene):polystyrene sulfonate (PEDOT:PSS)/poly(9-vinlycarbazole) (PVK)/QDs/2,2′,2″-(1,3,5-benzenetriyl) *tris*-[1-phenyl-1H-benzimidazole] (TPBi)/LiF/Al, achieving a maximum EQE and luminance of 3.0% and 330 cd m^{-2}, respectively, which is much higher compared to the APQD LEDs without ligand exchange. Furthermore, we demonstrated the flexibility and generality of our ligand-exchange strategy by exploiting mixed halide ion pairs to tune the emission of the QDs and further to fabricate blue PeLEDs possessing a maximum EQE and luminance of 1.9% and 35 cd m^{-2}, respectively. The reported efficiencies for both green and blue PeLEDs in this work represent a major leap for the family of APQD materials and pave

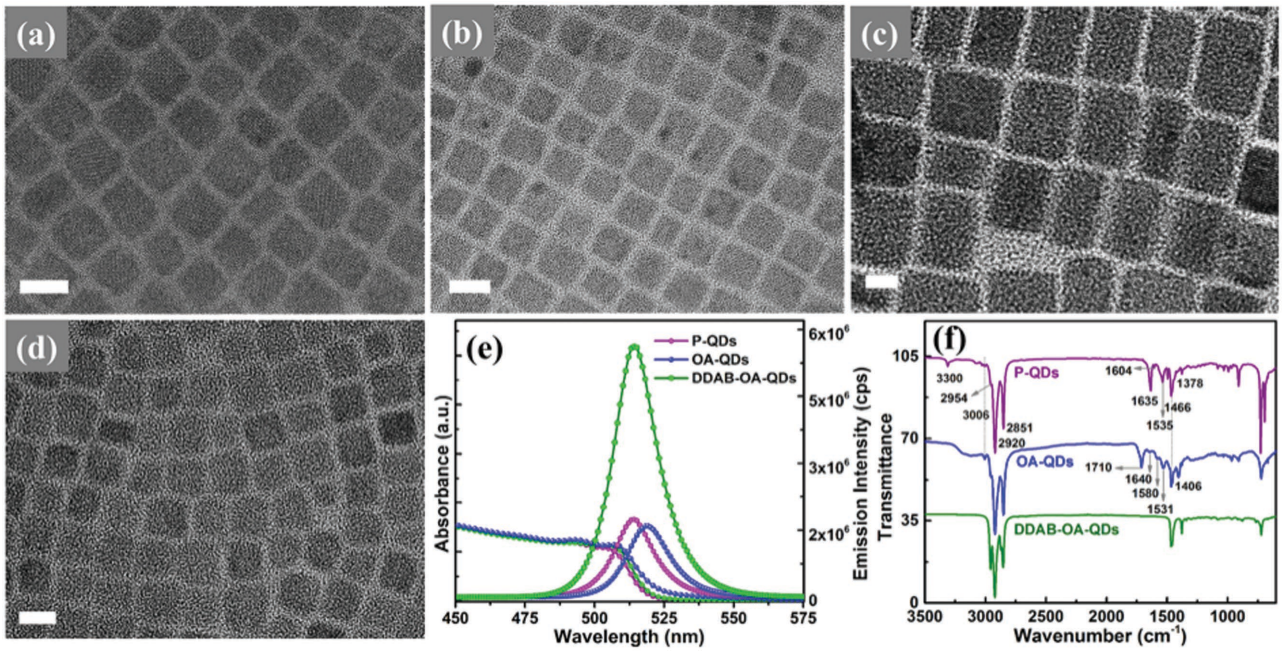

Figure 1. TEM images with scale bar of 10 nm: a) P-QDs without washing, b) OA-QDs, washed with butanol and dispersed in toluene, c) OA-QDs, washed with butanol after OA soaking for 30 min and dispersed in toluene, d) DDAB-OA-QDs, washed with butanol and dispersed in toluene, e) UV–vis absorption and PL spectra, and f) FTIR spectra of P-QDs, OA-QDs, DDAB-OA-QDs.

the way to further their exploitation in optoelectronics through judicious surface engineering.

The APQDs were synthesized via a modified hot-injection synthesis strategy by injecting cesium oleate into a $PbBr_2$ solution at 180 °C and stirring for 5 s.[24] The as-obtained reaction mixture containing QDs was quenched in an ice bath and purified for further treatment (see the Experimental Section for details). These purified QDs (herein referred as P-QDs) are soluble in nonpolar solvents such as toluene due to the presence of organic ligands (i.e., OA and OAm) on the QD surface. The solution of P-QDs/toluene exhibits a bright green color (see Figure S1, Supporting Information), which will turn into light brown immediately with the addition of OA, suggesting instability problems with the presence of excess OA and possible formation of large aggregates (the products were referred as OA-QDs). However, upon the introduction of DDAB in the final treatment step, a luminous bright green color reappeared (the products were referred to as DDAB-OA-QDs) (Figure S1, Supporting Information).

High-resolution transmission electron microscopy (TEM) was used to track the morphological changes during the treatment procedures. As shown in **Figure 1**a, the P-QDs are cubic shaped and monodisperse, with an average size of 10 nm (Figure 1a). The OA-QDs were washed with butanol and redispersed in toluene after removal of precipitates via centrifugation for TEM characterization. For the OA-QDs that were cleaned immediately after the addition of OA, TEM shows an increased average particle size (Figure 1b), while more obvious size increment can be observed if the QDs were kept with OA for 30 min before further cleaning (Figure 1c). However, the particle sizes and shapes can be preserved with immediate DDAB treatment after the addition of OA (Figure 1d). X-ray diffraction (XRD) confirmed the cubic crystal phase of all the samples, in accordance with previous reports (Figure S2, Supporting Information).[25,26]

Figure 1e shows the UV–visible absorption spectra of the QDs before (P-QDs) and after (DDAB-OA-QDs) ligand exchange. The close match of the two spectra implies that the size of QDs was preserved during ligand exchange. The enhanced PL intensity at 513 nm, along with the quantum yield increasing from 49% to 71% for DDAB-OA-QDs, indicates a better passivation of the surface trap states.[27] Notably, a 4 nm shift in PL spectra was noticed after OA treatment, possibly due to the adsorption of OA on the QD surface or the formation of slightly larger particles.

To elucidate the ligand-exchange process, Fourier transform infrared spectroscopy (FTIR) was used to examine the presence of ligand types in the as-synthesized and treated QD samples. As displayed in Figure 1f, all the samples show CH_2 and CH_3 symmetric and asymmetric stretching vibrations in the range of 2840–2950 cm^{-1}, and CH_2 bending vibration at 1466 cm^{-1}, which are the typical absorption bands for species with hydrocarbon groups.[28] The FTIR spectrum for the P-QDs sample shows an N–H stretching mode at 3300 cm^{-1}, indicating the presence of OAm on the P-QD surface.[29] The strong signal at 1635 cm^{-1} can be assigned to the asymmetric NH_3^+ deformation,[30] consistent with the appearance of N 1S at 401.8 eV in the X-ray photoelectron spectroscopy (XPS) analysis (discussed below). The absorptions at 1605, 1535, and 1406 cm^{-1} are ascribed to two asymmetric vibrations and one symmetric stretching vibration of the carboxylate group, indicating that oleate anions are complexed on the QD surfaces.[31,32] With the addition of OA, OAm gets protonated by excess protons, and further reacts with deprotonated OA to form an

Adv. Mater. 2016,
DOI: 10.1002/adma.201600784

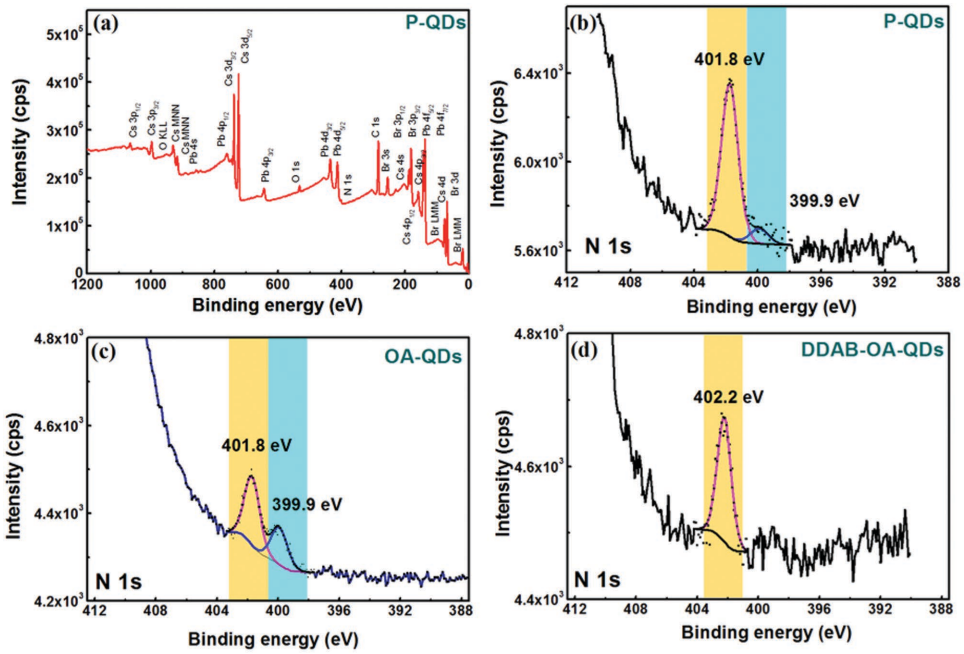

Figure 2. The X-ray photoelectron spectroscopy studies showing a) the survey spectrum of P-QDs and b–d) the high-resolution N 1s core-level spectra of P-QDs (b), OA-QDs (c), and DDAB-OA-QDs (d) (washed with butanol and dispersed in toluene).

acid–base complex, resulting in their desorption from the QD surface.[33,34] Subsequently, the excess OA adsorbs on the QD surfaces, as can be inferred from the emergence of the characteristic C=O stretching vibration band at 1710 cm^{-1} in the IR spectrum of the OA-QD sample.[35] To shed more light on the ligand-exchange process, we quantified the zeta potentials of various QD samples. In contrast with a negative value of –16 mV for the P-QDs, the OA-QDs shows a positive value of 10 mV, confirming the adsorption of OA on the QD surface and resulting in a polarity change. Such a scenario of protonation and desorption of OAm through the addition of OA has also been reported previously.[36,37]

However, both characteristic bands of N—H in OAm and C=O in OA disappear in the IR spectrum of the DDAB-OA-QDs, indicating a complete exchange of OA by DDAB on the QD surface. Such an exchange process may arise from the stronger affinity of Br^- ions to the positive sites (Pb^{2+} or Cs^+) on the QD surface compare to that of oleate group,[22,38] as well as the stronger affinity of DDA^+ with the negative sites (Br^-) or adsorbed Br^- on the QD surface. In addition, due to the larger steric hindrance of the branched structure of DDA^+, fewer DDA^+ ions may be adsorbed onto the QD surface, inducing a more negatively polarized QD due to the Br-rich surface,[39] which is confirmed by a zeta potential value of –60 mV. Such a large zeta potential along with the large steric hindrance of DDA^+ ensures a higher stability of the DDAB-OA-QD solution (Figure S3, Supporting Information). Such a passivation strategy, therefore, offers a solution to the instability problems caused by the highly dynamic binding of OAm and OA with the QDs,[34] so as to achieve a more stable ligand capping of the QDs through an X-type[22,23] binding using the ion pair ligand.

We also probed into the surface composition of all of the QD samples using XPS. The representative survey spectrum of P-QDs confirms the presence of Cs, Pb, Br, C, N, and O elements (**Figure 2**a).[39] No significant changes were observed for the Cs 3d, Pb 4f, Br 3d core levels spectra for the three samples (Figure S4, Supporting Information), yet the high-resolution spectra of the N 1s core level obtained from the three samples show noticeable changes (Figure 2b–d). The N 1s core level for P-QDs was fitted with two components at 399.9 and 401.8 eV. The dominant peak at 401.8 eV corresponds to protonated amine groups ($-NH_3^+$) while the peak at 399.9 eV is attributed to amine groups.[40,41] The N 1s core level for OA-QDs was fitted with similar components with reduced intensity. The existence of two N 1s core level suggested several equilibria from ammonium to amine that could exist.[34] However, the N 1s core level for DDAB-OA-QDs was fitted with a single peak at 402.2 eV corresponding to *tert*-ammonium cations from didodecyl dimethylammonium bromide.[42,43]

Combining the above analysis, we hypothesize that the acidic protons facilitate the removal of the OAm ligand by protonation. The protonated OAm ligands subsequently form acid–base complex with deprotonated OA groups,[36,37] and promote the coordination of the Br^- anions with the positively charged surface metal centers (Cs^+ or Pb^{2+}), as schematically illustrated in **Figure 3**, while the existence of DDA^+ on the QD surface helps to maintain their solubility in toluene. It is important to note that the intermediate process of adding excess amount of OA ligands in our two-step ligand-exchange procedure is vital to avoid the formation of 2D quantum wells of $(OAm)PbBr_4$ (Figure S5, Supporting Information),[44] likely through a protonation salt formation process. This is further confirmed by the time-dependent decrement in PL intensity of the as-synthesized P-QDs (Figure S6, Supporting Information) and clear morphological change from well-defined cubic shapes to larger plate-like structures (Figure S7, Supporting Information).

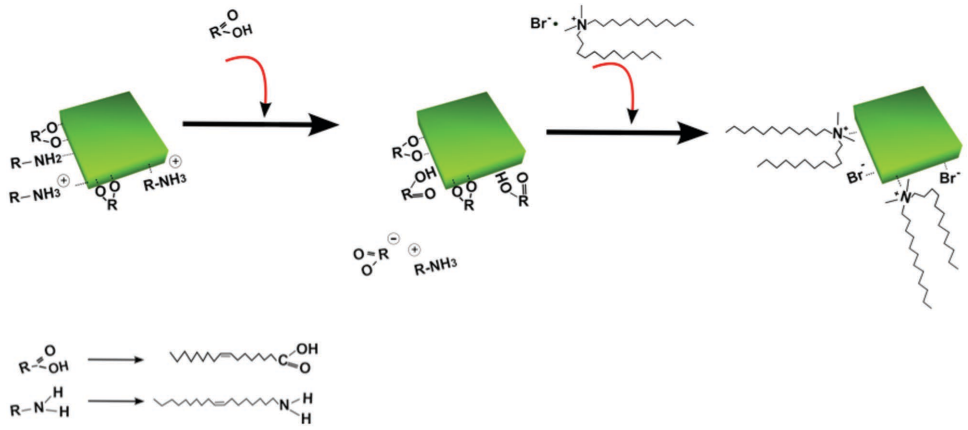

Figure 3. The ligand-exchange mechanism on $CsPbBr_3$ QD surfaces.

The surface morphology of the spin-coated thin films of P-QDs and DDAB-OA-QDs exhibit the densely packed surfaces over larger areas (Figure S8, Supporting Information). The P-QDs film showed larger grains compared to the DDAB-OA-QDs films further confirming the effect of surface-treatment in stabilizing the QDs. More importantly, the smoother films obtained in the case of DDAB-OA-QDs samples can correspond to the passivation of surface trap states as observed from the UV–vis absorption spectra. The absorbance measurements carried out on QDs used for device fabrication are shown in **Figure 4**. Bandgaps estimated from the Tauc plots (Figure 4a inset) showed a slight change of 0.04 eV upon treatment with OA and DDAB. The energy levels (conduction/valence band) estimated from the photoelectron spectroscopy (PESA) measurement and bandgaps respectively shown in Figure 4b are of interest for optoelectronic engineering of PeLEDS. These all-inorganic PeLED devices were characterized using the cross-section TEM (Figure 4c) where the multiple layers are arranged in the sequential order: ITO, PEDOT:PSS, 40 nm, PVK, 20 nm, perovskite QDs (8 nm), TPBi, 42 nm, and LiF/Al (10/100 nm). PVK is used as a hole-transporting and electron-blocking layer while TPBi is employed as an electron-transporting layer. The PVK layer reduces the hole-injection barrier, blocks the electrons in the active layer, and hence allow the holes and

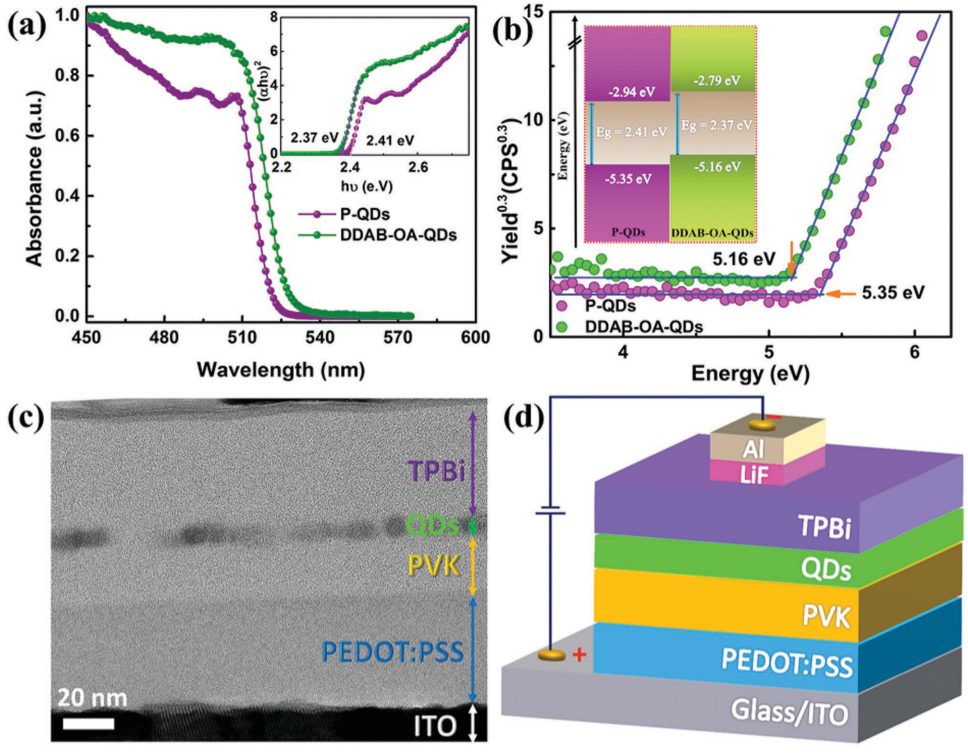

Figure 4. a) The thin-film absorption spectra with inset showing the Tauc plot for bandgap estimations of P-QDs and DDAB-OA-QDs. b) Photoelectron spectroscopy in air studies carried out for valence-band maximum (VBM). Inset showing the energy levels that are expressed from the vacuum, which is set at zero. c) Cross-sectional TEM image showing the multiple layers. d) Illustration of the schematic PeLED device structure.

Adv. Mater. **2016**,
DOI: 10.1002/adma.201600784

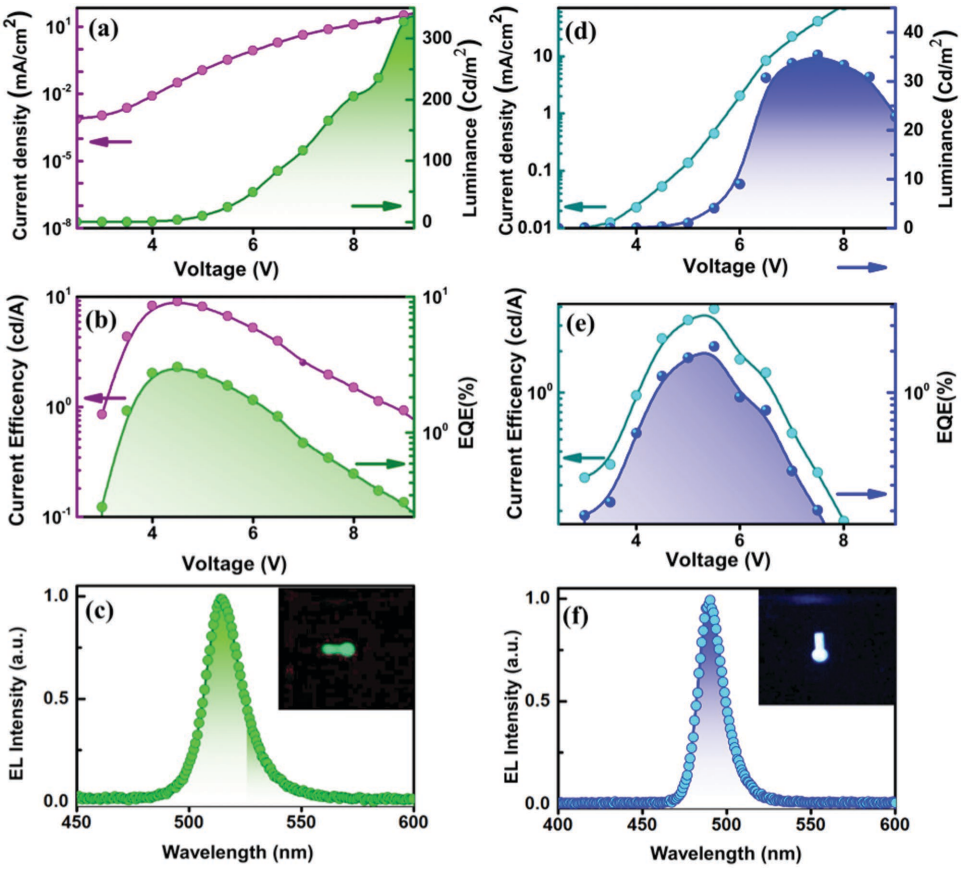

Figure 5. Green ($CsPbBr_3$) PeLED device performance. a) Current density and luminance versus driving voltage characteristics. b) Current efficiency and external quantum efficiency versus driving voltage characteristics. c) EL spectrum at an applied voltage of 4.5 V, and inset, a photograph of a device. Blue ($CsPbBr_3Cl_{3-x}$) PeLED device performance. d) Current density and luminance versus driving voltage characteristics. e) Current efficiency and external quantum efficiency versus driving voltage characteristics. f) EL spectrum at an applied voltage of 5.5 V, and inset, a photograph of a device.

electrons to recombine effectively in the QD emitting layer.[21] The complete device architecture used for the current study is shown schematically in Figure 4d.

The current-density–luminance–voltage (*J–L–V*) characteristic of the PeLEDs based on the typical green $CsPbBr_3$ QDs (DDAB-OA-QDs) is presented in **Figure 5**a. The turn-on voltage for the PeLED device is 3.0 V, lower than that of the PeLED based on untreated QDs (P-QDs) as emitting layer (Figure S9, Supporting Information), indicating that an efficient, barrier-free charge injection into the QD emitters was achieved.[45,46] And the better charge transport in the treated quantum-dot films was confirmed through a simple conductivity measurement (see details in Figure S10, Supporting Information). The luminance intensifies as the voltage increases, achieving the maximum value of 330 cd m^{-2} under a forward bias of 9 V. The current efficiency and EQE as a function of voltage for a typical green PeLEDs are shown in Figure 5b. A maximum EQE of 3.0% was reached at a voltage of 4.5 V, which is much higher than the maximum efficiency of control device using P-QDs as emitting layer (Figure S9, Supporting Information), and even higher than the reported value in the literature for all inorganic perovskite green LEDs.[21,46–48] The large enhancement in EQE indicates that the charge carrier balance in the QDs layer was significantly improved due to the use of halide-ion-pair ligands for passivation. The normalized electroluminescence spectrum (EL) of the QLEDs is shown in Figure 5c. The device gives an emission peak at 515 nm with a very narrow emission peak with full-width wavelength at half maximum (FWHM) of 19 nm, which is attributed to the narrow band-edge emission of QDs with a slightly redshifted emission compared with the PL spectrum acquired from the QD solution. Strikingly, the parasitic emission originated from the charge-transport layers (i.e., TPBi or PVK) was undetectable in the entire EL spectrum under various voltages, indicating good electron and hole blocking functions of both PVK and TPBi layers. The devices emit bright and uniform green light from the whole pixel under a bias of 5 V as shown in the inset in Figure 5c.

The blue PeLED devices were fabricated by using the same architecture of ITO/PEDOT:PSS/PVK/QDs/TPBi/LiF/Al, wherein the blue QDs were fabricated via an anion exchange strategy[49,50] by treating the P-QDs with a mixed halide-ion-pair ligand (di-dodecyl dimethyl ammonium bromide chloride, see the Experimental Section). The *J–L–V* characteristic of the blue PeLEDs ($CsPbBr_xCl_{3-x}$) is presented in Figure 5d. The turn-on voltage (calculated at a luminance of 1 cd m^{-2}) required for the blue PeLED device is 3.0 V, lower than the previous reported PeLED value,[21] also employing an efficient and barrier-free charge injection into the QD emitters.[45,46]

The electroluminescence intensifies as the voltage is increased, which leads to the maximum value of 35 cd m^{-2} under the applied voltage of 7.5 V. A maximum EQE of 1.9% has been reached under the applied voltage of 5.5 V (Figure 5e). The performance of these APQD LEDs can be further optimized in the future by controlling the crystal phase, balancing charge transport, improving PL efficiency, as well as by other short ligand replacement. The normalized EL spectra of blue PeLEDs with emission wavelength peaks at 490 nm (FWHM = 19 nm) is shown in Figure 5f. The devices exhibited a saturated and pure color as shown in the insert image of Figure 5f.

To better understand the role of the ligand treatments, transient photocurrent measurements were carried out on simple ITO/QDs/Au devices (Figure S11a, Supporting Information). The devices were held under dark and were optically excited using a 200 mW high-power LED source. The transient currents were recorded over 200 µs response times. Turn-on dynamics were monitored for current reaching the steady-state in both controlled and treated samples as a function of illumination light intensity. The shape of rise curves followed the light intensity dependence, providing clear evidence of trapping and detrapping mechanisms in both samples[51] (Figure S11b,c, Supporting Information). However, in comparison, the transient IV traces of treated samples reached the steady-state condition faster than control samples (Figure S11d, Supporting Information). A biexponential fitting revealed the faster and slower rise constants, where the controlled samples exhibited doubled values compared with treated samples (Figure S12, Supporting Information). These observations clearly suggest more defects and poor crystallinity in control samples compared to the treated samples.[52]

In summary, we have demonstrated a two-step ligand-exchange process for passivating $CsPbX_3$ (X = Br, Cl) QDs with halide and mixed halide ion pairs. Blue and green PeLEDs based on the passivated $CsPbX_3$ QDs displayed a sharp EL peak (FWHM = 19 nm) with a maximum luminance of 35 cd m^{-2} for the blue and 330 cd m^{-2} for the green, and high EQE (1.9% for the blue, and 3.0% for the green) for all-inorganic lead halide perovskites. The resultant PeLEDs' performance demonstrates that complete ligand exchanges by desorption of protonated OAm and subsequent treatment with a halide-ion-pair ligand improves charge carrier balance and device EQE. Our findings pave the way for the development of PeLEDs of high EQE and high luminescence based on stable inorganic perovskite QDs.

Experimental Section

Materials: 1-Butanol (BuOH, HPLC grade), was purchased from Fisher Scientific. Oleic acid (technical grade 90%), lead bromide ($PbBr_2$, 98%), and octane (98%) were purchased from Alpha Aesar. Cesium carbonate (Cs_2CO_3, 99.995%, metal basis), didodecyldimethylammonium chloride (DDAC, 98%), DDAB, 98%, OAm, technical grade 70%, and octadecene (ODE), technical grade 90% were purchased from Sigma-Aldrich. Toluene (HPLC grade) was purchased from Honeywell Burdick & Jackson. All chemicals were used as procured without further purification.

Preparation of Cesium Oleate Solution: Cs_2CO_3 (0.814 g) was loaded into 100 mL 2-neck flask along with ODE (30 mL) and oleic acid (2.5 mL), dried for 1 h at 120 °C, and then heated under N_2 to 160 °C until all Cs_2CO_3 reacted with OA. The solution was kept at 160 °C to avoid solidification before injection.

Synthesis and Purification of $CsPbBr_3$ QDs:[24] 100 mL of ODE, 10 mL of OAm, 10 mL of OA, and $PbBr_2$ (1.38 g) were loaded into a 250 mL flask, degassed at 120 °C for 30 min and heated to 180 °C under nitrogen flow. 8 mL of cesium oleate solution (0.08 M in ODE) was quickly injected. After 5 s, the reaction mixture was cooled using an ice-water bath. The crude solution was directly centrifuged at 8000 rpm for 10 min, the precipitate was collected and dispersed in toluene. One more centrifugation was required for purifying the final QDs.

Treatment of $CsPbBr_3$ QDs: 1 mL of the purified $CsPbBr_3$ QDs (15 mg mL^{-1}), 50 µL of OA was added under stirring, then added 100 µL DDAB toluene solution (0.05 M). The mixture solution was precipitated with BuOH after centrifugation and redissolved in 2 mL of octane. For the blue QDs ($CsPbBr_xCl_{3-x}$), a similar treatment procedure was applied except a mixed halide-ion-pair ligand (3 mL 0.005 M KBr aqueous solution mixed with 3 mL 0.05 M DDAC toluene solution, top layer solution was collected after centrifugation).

Device Fabrication: PEDOT:PSS solutions (Clevios PVP AI4083, filtered through a 0.45 µm filter) were spin-coated onto the ITO-coated glass substrates at 4000 rpm for 60 s and baked at 140 °C for 15 min. The hole transporting and electron blocking layer were prepared by spin-coating PVK chlorobenzene solution (concentration: 6 mg mL^{-1}) at 4000 rpm for 60 s. Perovskite QDs were deposited by spin-coating at 2000 rpm for 60 s in air. TPBi (40 nm) and LiF/Al electrodes (1 nm/100 nm) were deposited using a thermal evaporation system through a shadow mask under a high vacuum of 2×10^4 Pa. The device active area was 6.14 mm^2 as defined by the overlapping area of the ITO and Al electrodes. All the device tests were done under ambient condition.

Characterization: UV–vis absorption spectra were obtained using an absorption spectrophotometer from Ocean Optics. Carbon, hydrogen, oxygen, and sulfur analysis was performed using a Flash 2000 elemental analyzer (Thermo Fischer Scientific). Photoluminescence was tested using an FLS920 dedicated fluorescence spectrometer from Edinburgh Instruments. Quantum yield was measured using an Edinburgh Instruments integrating sphere with an FLS920-s fluorescence spectrometer. Fourier transform infrared spectroscopy (FTIR) was performed using a Nicolet 6700 FT-IR spectrometer. Powder X-ray diffraction patterns were recorded using Siemens diffractometer with Cu K_α radiation (λ = 1.54178 Å). Transmission electron microscopy (TEM) analysis was carried out with a Titan TEM (FEI Company) operating at a beam energy of 300 keV and equipped with a Tridiem postcolumn energy filter (Gatan, IQD.). The scanning electron microscopy (SEM) investigations were carried out on the Carl Zeiss, Gemini column field-emission SEM. Photoelectron spectroscopy measurements were carried out on the thin-film samples, using a Riken Photoelectron Spectrometer (Model AC-2). The power number was set at 0.3. XPS studies were carried out in a Kratos Axis Ultra DLD spectrometer equipped with a monochromatic Al K_α X-ray source ($h\nu$ = 1486.6 eV) operating at 150 W, a multichannel plate and delay line detector under 1.0×10^{-9} Torr vacuum. Measurements were performed in hybrid mode using electrostatic and magnetic lenses, and the take-off angle (angle between the sample surface normal and the electron optical axis of the spectrometer) was 0°. All spectra were recorded using an aperture slot of 300 µm × 700 µm. The survey and high-resolution spectra were collected at fixed analyzer pass energies of 160 and 20 eV, respectively. Samples were mounted in floating mode in order to avoid differential charging.[53] Charge neutralization was required for all samples. Binding energies were referenced to the C 1s peak (set at 284.8 eV) of the sp^3 hybridized (C–C) carbon from oleylamine and oleic acid. The data were analyzed with commercially available software, CasaXPS. The individual peaks were fitted by a Gaussian(70%)–Lorentzian (30%) (GL30) function after linear or Shirley-type background subtraction. The EL spectra and luminance (*L*)–current-density (*J*)–voltages (*V*) characteristics were collected by using a Keithley 2400 source, a calibrated luminance meter (Konica Minolta LS-110), and a PR-705 SpectraScan spectrophotometer (Photo Research) in the air and at room temperature. Zeta potential measurements were performed using a Zetasizer Nano-ZS (Malvern

Adv. Mater. 2016,
DOI: 10.1002/adma.201600784

Instruments). Each sample was measured five times and the average data was presented. Transient photocurrent measurements were performed under dark conditions using Paios system equipped with a white pulsed LED source with pulse length range 1 μs–5 s, and rise and fall time of the LED is 100 ns. The light Intensity at the device was measured as 2 kW m^{-2} in the spectral width of 350–700 nm.

Supporting Information

Supporting Information is available from the Wiley Online Library or from the author.

Acknowledgements

J.P., L.N.Q., and Y.Z. contributed equally to this work. This publication is based in part on Awards KUS-11-009-21 and URF/1/2268-01-01 made by King Abdullah University of Science and Technology (KAUST), by the Ontario Research Fund Research Excellence Program, and by the Natural Sciences and Engineering Research Council (NSERC) of Canada. L. N. Quan and D. H. Kim acknowledge the financial support by the National Research Foundation of Korea Grant funded by the Korean Government (Grant No. 2014R1A2A1A09005656). The authors acknowledge Mrs. Nini Wei and Dr. Jun Li for TEM cross-sections.

Received: February 9, 2016
Revised: July 10, 2016
Published online:

[1] M. M. Lee, J. Teuscher, T. Miyasaka, T. N. Murakami, H. J. Snaith, *Science* **2012**, *338*, 643.
[2] J. Luo, J. H. Im, M. T. Mayer, M. Schreier, M. K. Nazeeruddin, N. G. Park, S. D. Tilley, H. J. Fan, M. Grätzel, *Science* **2014**, *345*, 1593.
[3] N. J. Jeon, J. H. Noh, W. S. Yang, Y. C. Kim, S. Ryu, J. Seo, S. I. Seok, *Nature* **2015**, *517*, 476.
[4] G. Xing, N. Mathews, S. S. Lim, N. Yantara, X. Liu, D. Sabba, M. Grätzel, S. Mhaisalkar, T. C. Sum, *Nat. Mater.* **2014**, *13*, 476.
[5] B. R. Sutherland, S. Hoogland, M. M. Adachi, C. T. O. Wong, E. H. Sargent, *ACS Nano* **2014**, *8*, 10947.
[6] H. Zhu, Y. Fu, F. Meng, X. Wu, Z. Gong, Q. Ding, M. V. Gustafsson, M. T. Trinh, S. Jin, X. Y. Zhu, *Nat. Mater.* **2015**, *14*, 636.
[7] L. Dou, Y. Yang, J. You, Z. Hong, W. H. Chang, G. Li, Y. Yang, *Nat. Commun.* **2014**, *5*, 5404.
[8] S. Zhuo, J. Zhang, Y. Shi, Y. Huang, B. Zhang, *Angew. Chem., Int. Ed.* **2015**, *54*, 5693.
[9] G. Maculan, A. D. Sheikh, A. L. Abdelhady, M. I. Saidaminov, M. A. Haque, B. Murali, E. Alarousu, O. F. Mohammed, T. Wu, M. O. Bakr, *J. Phys. Chem. Lett.* **2015**, *6*, 3781.
[10] S. D. Stranks, H. J. Snaith, *Nat. Nanotechnol.* **2015**, *10*, 391.
[11] X. Dai, Z. Zhang, Y. Jin, Y. Niu, H. Cao, X. Liang, L. Chen, J. Wang, X. Peng, *Nature* **2014**, *515*, 96.
[12] B. S. Mashford, M. Stevenson, Z. Popovic, C. Hamilton, Z. Zhou, C. Breen, J. Steckel, V. Bulovic, M. Bawendi, S. Coe-Sullivan, P. T. Kazlas, *Nat. Photonics* **2013**, *7*, 407.
[13] Y. Yang, Y. Zheng, W. Cao, A. Titov, J. Hyvonen, R. MandersJesse, J. Xue, P. H. Holloway, L. Qian, *Nat. Photonics* **2015**, *9*, 259.
[14] Z. K. Tan, R. S. Moghaddam, M. L. Lai, P. Docampo, R. Higler, F. Deschler, M. Price, A. Sadhanala, L. M. Pazos, D. Credgington, F. Hanusch, T. Bein, H. J. Snaith, R. H. Friend, *Nat. Nanotechnol.* **2014**, *9*, 687.
[15] G. Li, Z. K. Tan, D. Di, M. L. Lai, L. Jiang, J. H. W. Lim, R. H. Friend, N. C. Greenham, *Nano Lett.* **2015**, *15*, 2640.
[16] H. Cho, S.-H. Jeong, M.-H. Park, Y.-H. Kim, C. Wolf, C.-L. Lee, J. H. Heo, A. Sadhanala, N. Myoung, S. Yoo, S. H. Im, R. H. Friend, T.-W. Lee, *Science* **2015**, *350*, 1222.
[17] M. Kulbak, D. Cahen, G. Hodes, *J. Phys. Chem. Lett.* **2015**, *6*, 2452.
[18] A. Dualeh, P. Gao, S. I. Seok, M. K. Nazeeruddin, M. Grätzel, *Chem. Mater.* **2014**, *26*, 6160.
[19] T. Baikie, Y. Fang, J. M. Kadro, M. Schreyer, F. Wei, S. G. Mhaisalkar, M. Graetzel, T. J. White, *J. Mater. Chem. A* **2013**, *1*, 5628.
[20] L. Protesescu, S. Yakunin, M. I. Bodnarchuk, F. Krieg, R. Caputo, C. H. Hendon, R. X. Yang, A. Walsh, M. V. Kovalenko, *Nano Lett.* **2015**, *15*, 3692.
[21] J. Song, J. Li, X. Li, L. Xu, Y. Dong, H. Zeng, *Adv. Mater.* **2015**, *27*, 7162.
[22] J. Tang, K. W. Kemp, S. Hoogland, K. S. Jeong, H. Liu, L. Levina, M. Furukawa, X. Wang, R. Debnath, D. Cha, K. W. Chou, A. Fischer, A. Amassian, J. B. Asbury, E. H. Sargent, *Nat. Mater.* **2011**, *10*, 765.
[23] Z. Ning, O. Voznyy, J. Pan, S. Hoogland, V. Adinolfi, J. Xu, M. Li, A. R. Kirmani, J.-P. Sun, J. Minor, K. W. Kemp, H. Dong, L. Rollny, A. Labelle, G. Carey, B. Sutherland, I. Hill, A. Amassian, H. Liu, J. Tang, O. M. Bakr, E. H. Sargent, *Nat. Mater.* **2014**, *13*, 822.
[24] J. Pan, S. P. Sarmah, B. Murali, I. Dursun, W. Peng, M. R. Parida, J. Liu, L. Sinatra, N. Alyami, C. Zhao, E. Alarousu, T. K. Ng, B. S. Ooi, O. M. Bakr, O. F. Mohammed, *J. Phys. Chem. Lett.* **2015**, *6*, 5027.
[25] C. C. Stoumpos, C. D. Malliakas, J. A. Peters, Z. Liu, M. Sebastian, J. Im, T. C. Chasapis, A. C. Wibowo, D. Y. Chung, A. J. Freeman, B. W. Wessels, M. G. Kanatzidis, *Cryst. Growth Des.* **2013**, *13*, 2722.
[26] Y. Bekenstein, B. A. Koscher, S. W. Eaton, P. Yang, A. P. Alivisatos, *J. Am. Chem. Soc.* **2015**, *137*, 16008.
[27] A. Nag, M. V. Kovalenko, J.-S. Lee, W. Liu, B. Spokoyny, D. V. Talapin, *J. Am. Chem. Soc.* **2011**, *133*, 10612.
[28] X. Lu, H.-Y. Tuan, J. Chen, Z.-Y. Li, B. A. Korgel, Y. Xia, *J. Am. Chem. Soc.* **2007**, *129*, 1733.
[29] A. S. M. Chong, X. S. Zhao, *J. Phys. Chem. B* **2003**, *107*, 12650.
[30] H. Y. Huang, R. T. Yang, D. Chinn, C. L. Munson, *Ind. Eng. Chem. Res.* **2003**, *42*, 2427.
[31] O. Bixner, A. Lassenberger, D. Baurecht, E. Reimhult, *Langmuir* **2015**, *31*, 9198.
[32] L. M. Bronstein, X. Huang, J. Retrum, A. Schmucker, M. Pink, B. D. Stein, B. Dragnea, *Chem. Mater.* **2007**, *19*, 3624.
[33] R. A. Harris, P. M. Shumbula, H. van der Walt, *Langmuir* **2015**, *31*, 3934.
[34] J. De Roo, M. Ibáñez, P. Geiregat, G. Nedelcu, W. Walravens, J. Maes, J. C. Martins, I. Van Driessche, M. V. Kovalenko, Z. Hens, *ACS Nano* **2016**, *10*, 2071.
[35] K. Yang, H. Peng, Y. Wen, N. Li, *Appl. Surf. Sci.* **2010**, *256*, 3093.
[36] S. B. Kim, C. Cai, J. Kim, S. Sun, D. A. Sweigart, *Organometallics* **2009**, *28*, 5341.
[37] A. Dong, X. Ye, J. Chen, Y. Kang, T. Gordon, J. M. Kikkawa, C. B. Murray, *J. Am. Chem. Soc.* **2011**, *133*, 998.
[38] J. S. Owen, J. Park, P.-E. Trudeau, A. P. Alivisatos, *J. Am. Chem. Soc.* **2008**, *130*, 12279.
[39] X. Li, Y. Wu, S. Zhang, B. Cai, Y. Gu, J. Song, H. Zeng, *Adv. Funct. Mater.* **2016**, *26*, 2584.
[40] B. Liao, P. Long, B. He, S. Yi, B. Ou, S. Shen, J. Chen, *J. Mater. Chem. C* **2013**, *1*, 3716.
[41] D. Q. Yang, M. Meunier, E. Sacher, *Appl. Surf. Sci.* **2005**, *252*, 1197.
[42] M. S. Bakshi, S. Sachar, G. Kaur, P. Bhandari, G. Kaur, M. C. Biesinger, F. Possmayer, N. O. Petersen, *Cryst. Growth Design* **2008**, *8*, 1713.
[43] Y. Leng, Y. Li, A. Gong, Z. Shen, L. Chen, A. Wu, *Langmuir* **2013**, *29*, 7591.
[44] I. Koutselas, P. Bampoulis, E. Maratou, T. Evagelinou, G. Pagona, G. C. Papavassiliou, *J. Phys. Chem. C* **2011**, *115*, 8475.

[45] W. K. Bae, Y. S. Park, J. Lim, D. Lee, L. A. Padilha, H. McDaniel, I. Robel, C. Lee, J. M. Pietryga, V. I. Klimov, *Nat. Commun.* **2013**, *4*, 2661.
[46] X. Zhang, H. Lin, H. Huang, C. Reckmeier, Y. Zhang, W. C. H. Choy, A. L. Rogach, *Nano Lett.* **2016**, *16*, 1415.
[47] N. Yantara, S. Bhaumik, F. Yan, D. Sabba, H. A. Dewi, N. Mathews, P. P. Boix, H. V. Demir, S. Mhaisalkar, *J. Phys. Chem. Lett.* **2015**, *6*, 4360.
[48] G. Li, F. W. R. Rivarola, N. J. L. K. Davis, S. Bai, T. C. Jellicoe, F. de la Peña, S. Hou, C. Ducati, F. Gao, R. H. Friend, N. C. Greenham, Z.-K. Tan, *Adv. Mater.* **2016**, *28*, 3528.
[49] Q. A. Akkerman, V. D'Innocenzo, S. Accornero, A. Scarpellini, A. Petrozza, M. Prato, L. Manna, *J. Am. Chem. Soc.* **2015**, *137*, 10276.
[50] G. Nedelcu, L. Protesescu, S. Yakunin, M. I. Bodnarchuk, M. J. Grotevent, M. V. Kovalenko, *Nano Lett.* **2015**, *15*, 5635.
[51] Z. Li, F. Gao, N. C. Greenham, C. R. McNeill, *Adv. Funct. Mater.* **2011**, *21*, 1419.
[52] Y. Li, L. Meng, Y. Yang, G. Xu, Z. Hong, Q. Chen, J. You, G. Li, Y. Yang, Y. Li, *Nat. Commun.* **2016**, *7*, 10214.
[53] Y. Mori, M. Tanemura, S. Tanemura, *Appl. Surf. Sci.* **2004**, *228*, 292.

Adv. Mater. **2016**,
DOI: 10.1002/adma.201600784